

# Control of topological defects in microstructured liquid crystal cells

**G. Vijaya Prakash**

*Department of Physics, Indian Institute of Technology, New Delhi, India*

**M. Kaczmarek, A. Dyadyusha and J.J. Baumberg**

*School of Physics and Astronomy, University of Southampton, Southampton, SO17 1BJ*

**G. D'Alessandro**

*School of Mathematics, University of Southampton, Southampton, SO17 1BJ*

[dales@soton.ac.uk](mailto:dales@soton.ac.uk)

**Abstract:** We study how the propagation of light inside recently developed micro-structured cells, can be actively tuned by polarising the nanoscale defects in the nematic liquid crystals they contain. Our ‘planar-spherical’ cells are formed by assembling a planar and a gold-coated hemispherical micro-mirror. Optical reflection images of the back-reflected polarised light show a remarkable change of symmetry as a function of the voltage applied to the cell. Theoretical models of the alignment of the liquid crystal within the cell indicate that the constraints imposed on the liquid crystal by the cell geometry and by the applied electric field induces the formation of defects. Their motion under the effect of the applied electric field is responsible for the change of symmetry of the back-reflected light. Furthermore, experimental measurements of the relaxation time of the back-reflected intensity indicate that the motion of the defect in our micro-structured cells is much faster than in equivalent planar cells.

© 2005 Optical Society of America

**OCIS codes:** (160.3710) Liquid crystals; (230.3990) Microstructure devices; (240.0240) Optics at surfaces; (310.6860) Thin films, optical properties

---

## References and links

1. G. P. Crawford and S. Žumer, eds., *Liquid Crystals in Complex Geometries* (Taylor & Francis, London, 1996).
2. J. H. Erdmann, S. Žumer, and J. W. Doane, “Configuration Transition in a Nematic Liquid Crystal Confined to a Small Spherical Cavity,” *Phys. Rev. Lett.* **64**, 1907–1910 (1990).
3. V. Yu Reshetnyak, T. J. Sluckin, and S. J. Cox, “Effective medium theory of polymer dispersed liquid crystal droplet systems: II. Partially oriented bipolar droplets,” *J. Phys. D: Appl. Phys.* **30**, 3253–3266 (1997).
4. W. Y. Li and S. H. Chen, “Simulation of normal anchoring nematic droplets under electrical fields,” *Jap. J. Appl. Phys.* **1** **38**, 1482–1487 (1999).
5. M. Abbate, P. Mormile, E. Martuscelli, P. Musto, L. Petti, G. Ragosta, and P. Villano, “PDLC based on unsaturated polyester resins: molecular, morphological and thermo-optical analysis,” *J. Mat. Sci.* **35**, 999–1008 (2000).
6. S. C. Sharma, L. Zhang, A. J. Tapiawala, and P. C. Jain, “Evidence for droplet reorientation and interfacial charges in a polymer-dispersed liquid-crystal cell,” *Phys. Rev. Lett.* **87**, 105501(4) (2001).
7. O. Lavrentovich, “Topological defects in dispersed liquid crystals, or words and worlds around liquid crystal drops,” *Liq. Crys.* **24**, 117–125 (1998).
8. A. Fernández-Nieves, D. R. Link, D. Rudhardt, and D. A. Weitz, “Electro-Optics of Bipolar Nematic Liquid Crystal Droplets,” *Phys. Rev. Lett.* **92**, 105503(4) (2004).
9. T. Yamaguchi, Y. Kawata, and Y. Mori, “Boundary condition effects on field-induced deformation modes in polymer dispersed liquid crystals,” *Appl. Phys. Lett.* **72**, 1170–2 (1998).

10. P. Mach, P. Wiltzius, M. Megens, D. A. Weitz, K. H. Lin, T. C. Lubensky, and A. G. Yodanis, "Electro-optic response and switchable Bragg diffraction for liquid crystals in colloid-templated materials," *Phys. Rev. E* **65**, 031720(3) (2002).
11. D. W. Berreman, "Solid Surface Shape and the Alignment of an Adjacent Nematic Liquid Crystal," *Phys. Rev. Lett.* **28**, 1683–1686 (1972).
12. C. Rosenblatt, "Nanostructured surfaces: Scientific and optical device applications," *Mol. Cryst. Liq. Cryst.* **412**, 1727–1744 (2004).
13. T. Pfohl, J. H. Kim, M. Yasa, H. P. Miller, G. C. L. Wong, F. Bringezu, Z. Wen, L. Wilson, M. W. Kim, Y. Li, and C. R. Safinya, "Controlled Modification of Microstructured Silicon Surfaces for Confinement of Biological Macromolecules and Liquid Crystals," *Langmuir* **17**, 5343–5351 (2001).
14. M. Ibn-Elhaj and M. Schadt, "Optical polymer thin films with isotropic and anisotropic nano-corrugated surface topologies," *Nature* **410**, 796–799 (2001).
15. R. Penterman, S. I. Klink, H. de Koning, G. Nisato, and D. J. Broer, "Single-substrate liquid-crystal displays by photo-enforced stratification," *Nature* **417**, 55–58 (2002).
16. C. Schuller, F. Klopff, J. P. Reithmaier, M. Kamp, and A. Forchel, "Tunable photonic crystals fabricated in III-V semiconductor slab waveguides using infiltrated liquid crystals," *Appl. Phys. Lett.* **82**, 2767–9 (2003).
17. G. Mertens, T. Rošder, R. Schweins, K. Huber, and H. Kitzrow, "Shift of the photonic band gap in two photonic crystal liquid crystal composites," *Appl. Phys. Lett.* **80**, 1885–1887 (2002).
18. G. Vijaya Prakash, L. Besombes, T. Kelf, J. J. Baumberg, P. N. Bartlett, and M. E. Abdelsalam, "Tunable resonant optical microcavities by self-assembled templating," *Opt. Lett.* **29**, 1500–2 (2004).
19. S. Coyle, G. V. Prakash, J. J. Baumberg, M. Abdelsalam, and P. N. Bartlett, "Spherical micromirrors from templated self-assembly: Polarization rotation on the micron scale," *Appl. Phys. Lett.* **83**, 767–769 (2003).
20. A. Sonnet, A. Kilian, and S. Hess, "Alignment tensor versus director: Description of defects in nematic liquid crystals," *Phys. Rev. E* **52**, 718–722 (1995).
21. P. G. de Gennes and J. Prost, *The physics of liquid crystals*, 2nd ed. (Clarendon Press, Oxford, 1993).
22. R. Barberi, F. Ciuchi, G. E. Durand, M. Iovane, D. Sikharulidze, A. M. Sonnet, and E. G. Virga, "Electric field induced order reconstruction in a nematic cell," *Eur. Phys. J. E* **13**, 61–71 (2004).
23. C. Greenough, "The finite element library (felib)," (2001). URL <http://www.cse.clrc.ac.uk/msw/felib/felib-top.shtml>.
24. Liquicoat PA ZLI-3334 0.2% solution in ethanol (Merck).
25. T. G. Sokolovska, R. O. Sokolovskii, and G. N. Patey, "Surface-induced ordering of nematics in an external field: The strong influence of tilted walls," *Phys. Rev. Lett.* **92**, 185508(4) (2004).

## 1. Introduction

Ordering in nematic liquid crystals (LCs) has been subject to intensive research for now many years [1]. Two main configurations have been the focus of most effort: planar cells and polymer-dispersed liquid crystals (PDLCs). In the former, the liquid crystal is sandwiched between two plane surfaces. Electrical and optical functionality is achieved through torques on the molecules, which in turn resist through elastic forces and molecular anchoring at the interfaces (Fig. 1(a)). In the latter, birefringent spherical droplets of liquid crystal are included in a polymer matrix and contain defects that can be switched between several configurations (Fig. 1(b),(c)) [2, 3]. The type of defect, generally, depends on the size and shape of the droplets. The switching characteristics of PDLCs can be modified mainly through changes in the surface anchoring energy and the inter-molecular interactions [4, 5, 6]. The complex variety of behaviors [7] that surface anchoring or boundary conditions impose on the liquid crystals is not only evident in individual PDLC spheres or hexagonal droplets [8], but also in large, cylindrical, polymer cavities [9] and infiltrated opals [10]. The effect of confined geometries and surfaces on the behavior of liquid crystals can also be observed in planar cells with corrugated surfaces: for example, corrugations in two dimensions can lead to homeotropic alignment [11]. Complex surface interactions were studied in a variety of confined geometries: ridges [12, 13], two dimensional irregular patterns [14] or regular square lattices [15]. One of the goals of such studies was to demonstrate dramatic spectral tuning of periodically patterned photonic crystals infiltrated with LCs [16, 17]. However, this has proved very challenging, mainly due to the subtleties of the LC-surface interaction.

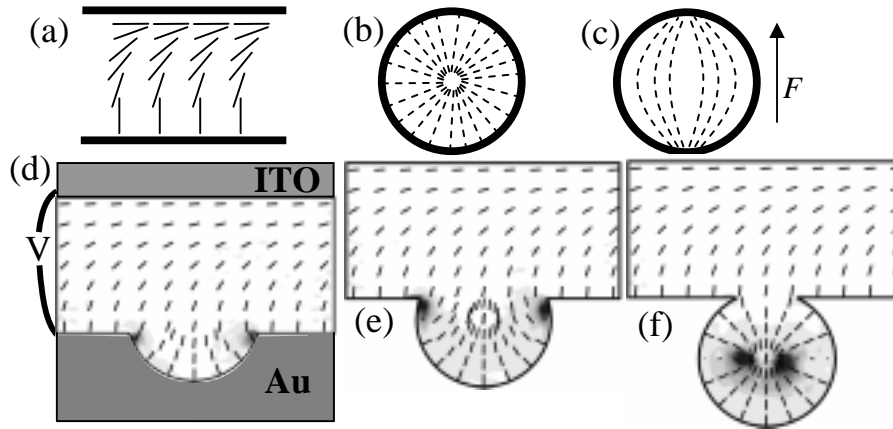


Fig. 1. Schematic liquid crystal alignment in (a) flat hybrid cell, (b,c) in spherical droplet at low/high electric field. (d) Microcavity cell geometry with contacts. (d-f) Liquid crystal cell geometries evolving between (a) and (b), with molecular alignment at 0V predicted by model (2). The shading indicates the magnitude of the scalar order parameter (darker shading corresponds to lower values).

## 2. The planar-spherical cell

In this paper we introduce an alternative and widely-configurable route to control liquid crystalline order. A 3D micro-scale architecture, the *planar-spherical cell*, is harnessed to influence the formation and dynamics of point defects. The resulting systems can be continuously tuned all the way from planar cells (typical of nematic display devices) to spherical voids (typical of polymer-dispersed liquid crystal devices). A model based on Landau-de Gennes theory shows that the constrained geometry can induce the formation of defects and that these can be altered and moved by an applied electric field. We confirm such behavior experimentally using specially micro-structured liquid crystal cells. Our experiments demonstrate that micron-scale spherical dishes display dynamically-controlled birefringence in their reflectivity. Such control of the molecular order using micro- and, eventually, nano-geometries opens an exciting prospect for a wide range of molecular functionality.

Our approach is to devise 3D microscale geometries which systematically morph from flat into spherical cavities (Fig. 1(d-f)). Using our recently developed micro-templating technology, spherical mirrors with radius of curvature from 100nm to 100 $\mu$ m can be produced [18]. This method is based on self-assembly of polyester microspheres on a gold substrate followed by electrochemical deposition of gold around them to any desired thickness [19]. Highly reflective metallic micromirrors with selectable aperture diameters  $D$  can be achieved by controlling the electrochemical deposition parameters. We have used spheres of diameter  $a = 5\mu$ m, although 10 $\mu$ m diameter give similar results, to prepare the micromirrors with graded thickness ranging from  $0.2a$  to almost a closed sphere (Fig. 2(a)-(d)).

## 3. Modeling the director field in a planar-spherical cell

In order to understand the effect of the electro-optic response on pre-aligned LCs inside the micromirror we have developed a model that gives the alignment tensor of the LCs in three dimensions coupled with an electrostatic field. We represent the LC director field in the cavity using a  $3 \times 3$  traceless symmetric tensor  $\mathcal{Q}$ . This field may be defined in terms of the unit vector

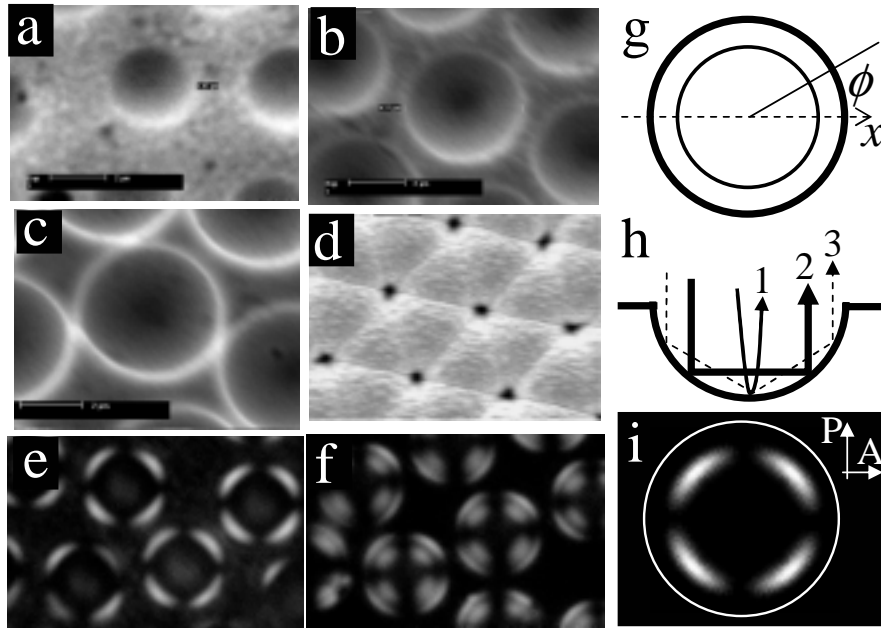


Fig. 2. (a-d) SEM images for  $2.5\mu$  radius of curvature Au surfaces grown to a thickness of  $0.8, 1.5, 2.5, 4.5 \mu\text{m}$  (giving apertures  $D=3.2, 4.2, 5, 0.8 \mu\text{m}$ ). (e, f) Cross-polarized optical reflection images of Au microdishes with  $D=4.2, 5\mu\text{m}$ . (h) Multiple bounce ray trajectories and (g) the two-bounce ring, with (i) its predicted cross-polarized reflectivity. The arrows indicate the direction of the polarizer (P) and of the analyzer (A).

$n$  that describes the average orientation of the liquid crystal molecules as [20]

$$Q_{ij} = \sqrt{\frac{3}{2}} S \left( n_i n_j - \frac{1}{3} \delta_{ij} \right) \equiv S \overline{n \otimes n} \quad (1)$$

where  $Q_{ij}$  is the  $(ij)$ -th component of  $\mathcal{Q}$  and  $S$  is the scalar order parameter of the director field. The equilibrium configuration of  $\mathcal{Q}$  is the minimum of a Landau-de Gennes free energy [21] that can be written in non-dimensional notation as [22]

$$\mathcal{F} = \frac{1}{2} \xi_0^2 |\nabla \mathcal{Q}|^2 + \frac{1}{2} \vartheta \text{Tr}(\mathcal{Q}^2) - \sqrt{6} \text{Tr}(\mathcal{Q}^3) + \frac{1}{2} \text{Tr}^2(\mathcal{Q}^2) - \chi_a \text{Tr}(\mathcal{Q} \mathcal{E}). \quad (2)$$

Here  $\xi_0$  is a diffusion length whose square is the scaling unit of the bending energy,  $\vartheta$  is a temperature ( $\vartheta = 0$  at the pseudo-critical point and  $\vartheta = 1$  at the clearing point) that measures the bulk energy of the nematic phase,  $\chi_a$  is the electro-static coupling constant and  $\mathcal{E} \equiv \overline{E \otimes E}$ , where  $E$  is the electrostatic field applied to the cavity. We have solved the dynamical equations that lead to the minimum of the free energy (2) in a given electrostatic field using the method of Ref. [20] coupled with a finite element Crank-Nicolson method based partially on the Felib library [23].

The liquid crystals are assumed to remain rigidly aligned at the boundaries. The electric field is solved exactly inside the non-planar geometry, but is assumed to remain independent of the evolving molecular alignment. Figures 1(d)-(f) show cross sections of the LC director alignment (dark lines) and of the scalar order parameter (gray-scale mapping) with no applied electric

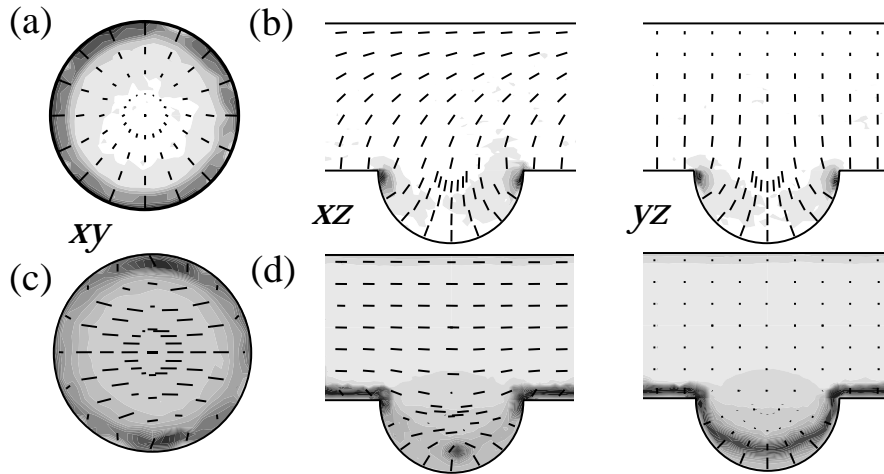


Fig. 3. Cross-sections showing simulated molecular director (orientation and order parameter  $S=1.7$  (white) to  $0.6$  (dark)) inside the microcavity for  $0V$  (a,b) and  $10V$  (c,d). (a,c) Plan views just below the rim, (b,d) side-view through microcavity center in  $xz$  and  $yz$  planes. The void diameter  $a$  is  $5\mu\text{m}$ .

field in three different cavity geometries. The alignment of the LC director is perpendicular to the surface on the lower, micro-patterned surface (homeotropic alignment) and parallel to the  $x$  (rubbing) direction on the top surface (planar alignment). In all simulations the liquid crystal has a negative dielectric susceptibility, with parameters  $\xi_0^2 = 1.6 \times 10^{-3}$ ,  $\vartheta = -0.36$ ,  $\chi_a = -0.02$ . It is worth noting that the alignment in Fig. 1(f) closely resembles the symmetry breaking of ‘hedgehog’ defects, previously found in spherical droplets [20] (see Fig. 1(b)).

Figure 3 illustrates an example of the effect of the applied electro-static field on the director configuration at two specific applied voltages. The images in Fig. 3(a),(c) are slices taken just below the rim of the spherical mirror, whereas Fig. 3(b),(d) shows cross sections along  $xz$  and  $yz$  planes.

At low applied field, the molecules continuously bend and twist from the bottom surface homeotropic alignment to the top surface planar alignment. As the applied field is increased, the molecules experience a torque that tends to align them orthogonally to the field lines and parallel to the rubbing direction. The scalar order parameter is also affected by the applied electric field: at low field intensity there is a reduction in the degree of molecular alignment in a ring around the top of the cavity, i.e., the order parameter  $S$  is locally reduced at the rim (darker area in Fig. 3(a)). At a critical applied field, a defect starts to form on the circumference at the location, where the bending of the liquid crystal is highest. As the field is increased further, this defect moves down inside the cavity, eventually resting at the bottom of the cavity (Fig. 3(d)). From a comparison of Figs. 3(b) and (d) it can be seen that the final configuration mixes aspects of both hedgehog and planar alignments of Fig. 1(a),(b). Our simulations thus indicate that the formation and control of defects can be achieved by combining a high curvature surface and a microcavity geometry.

#### 4. Experimental and numerical birefringence patterns from planar-spherical cells

The study of LC alignment through its birefringence effects on polarized light [21] is a very effective experimental technique. A sensitive ‘polarization signature’ is carried by light rays after their multiple bounces inside the spherical metallic cavity, as shown in Fig. 2(h) [19]. In our ex-

periments, the cavity is placed under a microscope and illuminated from the top by a collimated beam of polarized, white light. The light back-reflected from the bottom layer passes through a polarizer orthogonal to the incident polarization and is collected by the objective of the microscope. When a collimated beam of polarized white light hits the spherical surface, a geometric polarization rotation results. This leads to the pattern plotted in Fig. 2(i), when viewed through crossed polarizers and taken at high magnification (Fig. 2(e),(f)). Essentially only light with polarization either parallel or orthogonal to the spherical surface is unaffected by the geometric rotation and thus appears dark in cross polarizers, giving a four-lobed symmetry [19].

In our experiments the LC cells have, essentially, a substrate composed of arrays of the Au micromirrors and an ITO-coated glass plate on top (Fig. 1(e)). The top surface is prepared as for a hybrid cell: the ITO is coated with an ultra-thin layer of polyimide and mechanically rubbed in one direction ( $x$ ) to create a surface that aligns the LC with a pre-tilt angle of less than  $5^\circ$ . Similarly, the micromirror surface is treated with a surfactant [24] to produce homeotropic LC alignment. Latex spacers maintain a uniform cavity with a distance between the flat Au (outside the micromirrors) and the top ITO of  $10\mu\text{m}$ . In our present investigation, we used a negative dielectric susceptibility liquid crystal (Merck MLC-6608, birefringence  $\Delta n = 0.083$ ) to fill the cells by standard LC cell preparation procedures. Separately contacting the ITO and Au to a frequency source allows 1kHz AC electric fields,  $F_{ac}$ , to be applied across the cell. Summarizing, our LC cells have a geometry tunable from hybrid flat to spherical void which can be addressed with an external electrical field.

Once the cell is filled, the four-lobed reflection seen under cross-polarization persists (Fig. 4(a),(c)), providing that the incident optical field is polarized along or across the rubbing direction, i.e., along the  $x$  and  $y$ -axis respectively. As the electric field is increased the four-lobed pattern evolves gradually to a two-lobed pattern (Fig. 4(b),(d)) which persists up to 5V. The extra rotation of the polarization induced by the re-orientation of the LC only affects rays that reflect inside the micromirror in the direction perpendicular to the rubbing direction, while the beam bouncing along the rubbing direction remains unaltered. This contrasting behavior is independent of whether the polarization of the incident beam is along or across the rubbing direction.

To compare more carefully with the theoretical simulations, we measured under cross-polarizers the intensity of the rays back-reflected after two bounces (Fig. 2(g),(h)) as a function of the azimuthal angle  $\phi$  relative to the rubbing direction, for  $F_{ac}=0-5\text{V}$  (Fig. 4(e)). To obtain the corresponding theoretical curve, we tracked the two-bounce optical rays through the LC cell, accumulating the polarization rotation from birefringence along these paths (Fig. 4(f)). We assumed that the induced LC birefringence does not significantly perturb the ray directions from those of an empty cavity. This model, although approximate, gives results in qualitative agreement with the experimental data: the theoretical and experimental azimuthal traces show many similar features, including the reduction from 4-fold to 2-fold symmetry when the applied field is increased. More in-depth modeling will be the focus of future work.

We can glean an understanding of the polarization pattern observed at high applied voltage by looking at Fig. 3. An empty cell illuminated with linearly polarized light has four-fold symmetry, as illustrated in the intensity pattern of Fig. 2(e),(f). A filled cell has lower symmetry: the bulk part of the cell (the rectangular regions in Fig. 3(b),(d)) is symmetric just with respect to reflection along the  $x$ -axis, while, at low applied voltage, the spherical part of the cell has axial symmetry (Fig. 3(a)). The end result of the competition between these two symmetries is an intensity pattern with four-fold symmetry (Fig. 4(a),(c)) very similar to that observed in an empty cavity. When the intensity of the applied electric field is increased, a defect appears at the bottom of the spherical mirror; it removes the axial symmetry of the spherical cavity and replaces it with a symmetry with respect to the  $x$ -axis only (Fig. 3(c)). This loss of symmetry

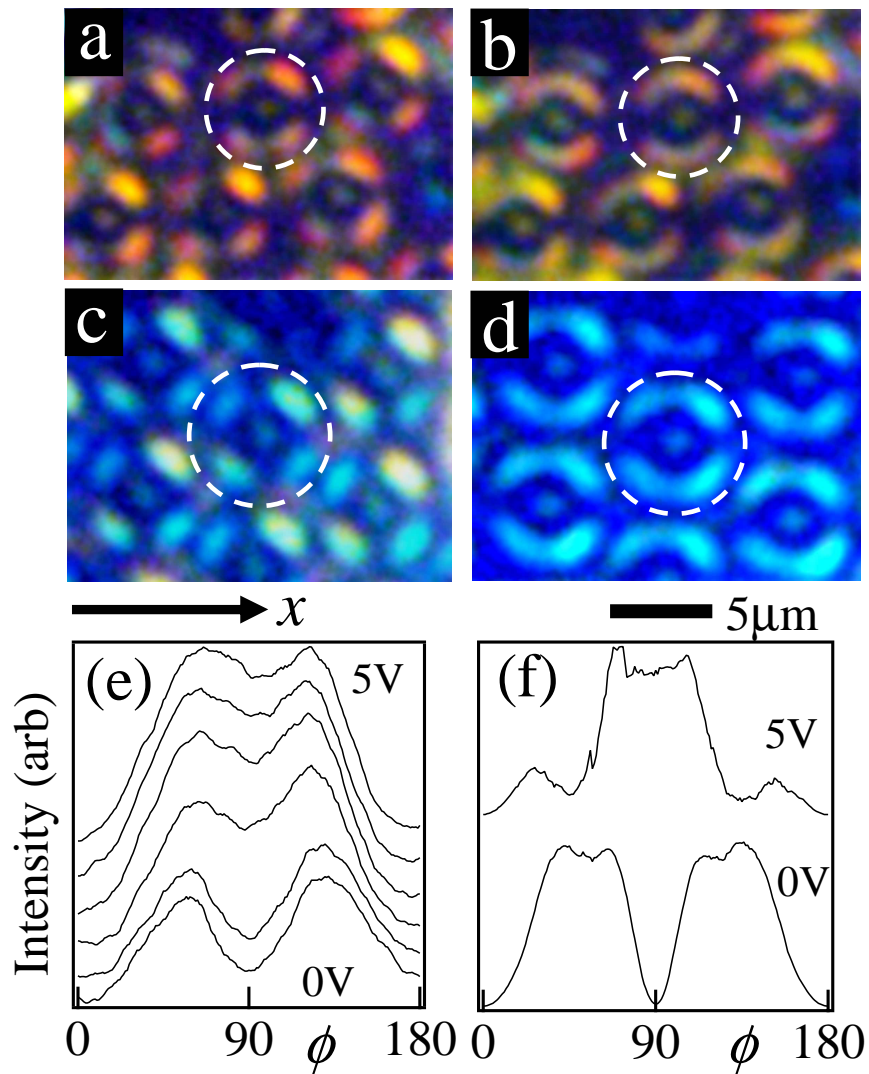


Fig. 4. Cross-polarized optical images of LC filled microdishes at 0V (a,c) and 5V (b,d) for (a,b) 1.5 $\mu$ m thick and (c,d) 2.5 $\mu$ m thick Au films. The arrow shows the rubbing direction (alignment on upper ITO). (e,f) Cross-polarized reflected intensity as a function of azimuthal angle  $\phi$  around the reflected ring, extracted from (e) experiment and (f) theory.

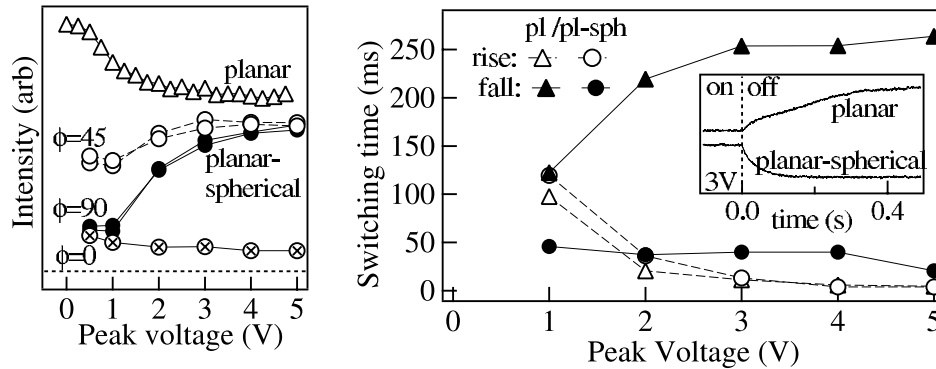


Fig. 5. (a) Applied-field dependent intensity of two-bounce cross-polarized reflectivity at  $\phi = 0^\circ, 45^\circ, 90^\circ$ , compared to the flat hybrid cell. The two traces for  $\phi = 45^\circ, 90^\circ$  represent the intensity measured clockwise and counter-clockwise with respect to the rubbing direction. (b) Rise and fall times of the light intensity at  $90^\circ$  in a planar-spherical microcavity and in a flat hybrid cell under square wave modulation. The insert shows the dynamical response of the two types of cavities when an applied 3V potential is switched off.

affects also the reflected light intensity, whose symmetry decreases from four-fold to two-fold (Fig. 4(b),(d)).

### 5. Experimental measurement of the defect switching times

To identify the role of geometry on the dynamics of the defects, we have experimentally measured the threshold and dynamics in LC microcavities and in flat cells (Fig. 5). Although the voltage *threshold* for field-induced molecular realignment is virtually unaffected, we observe very different *dynamics*. When the applied 1kHz AC field is turned on, both cells show a rise time which reduces as the amplitude increases (Fig. 5(b)). However, when the field is removed, the cells recover their initial state very differently, with fall times up to 10 times faster in the microcavity. In the flat cell, the further the molecules have been reoriented, the slower their recovery is (it more than doubles to 250ms). In the spherical microcavity, the further the defect has been displaced into the dish, the faster it subsequently moves back (halving to 25ms). This reflects the strong influence that the geometrical constraints have on the liquid crystal alignment inside the spherical cavity, a phenomenon that has striking similarities to the wall effect studied theoretically in [25]. Previous studies of response time in infiltrated opals (giving uncontrolled defects) suggested that a faster response was due to LC domain interconnectivity [10]. However, in our case there is only one defect per microcavity and, therefore, this explanation cannot apply. A more detailed theoretical modeling of the motion of the defects and of their dynamics will be the focus of future work.

### 6. Conclusions

In summary, we have used optical geometries that allow us to study the changes in a single defect, combining features of both plane and spherical LC cells. We have demonstrated theoretically and confirmed experimentally, that molecular alignment in 3D micro-geometries can lead to controllable, localized LC defects, which can be initiated and displaced by applied fields. These promising results are of great importance and relevance to a whole range of applications such as integrated modulators, as well as active photonic crystals (both 2D and 3D).

### **Acknowledgments**

We would like to thank T.J. Sluckin for helpful discussions and acknowledge Merck, DSTL, EPSRC GR/R54194, GR/A00155 and GR/R27235.